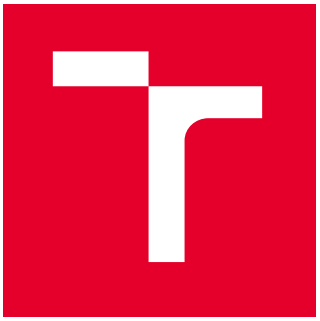

BRNO UNIVERSITY OF TECHNOLOGY

VYSOKÉ UČENÍ TECHNICKÉ V BRNĚ

CENTRAL EUROPEAN INSTITUTE OF TECHNOLOGY BUT

STŘEDOEVROPSKÝ TECHNOLOGICKÝ INSTITUT VUT

PREPARATION AND CHARACTERIZATION OF NANOSTRUCTURED III-V SEMICONDUCTOR MATERIALS

PŘÍPRAVA A CHARAKTERIZACE NANOSTRUKTURNÍCH III-V POLOVODIČOVÝCH MATERIÁLŮ

DOCTORAL THESIS
DIZERTAČNÍ PRÁCE

AUTHOR — **Ing. Jaroslav Maniš**
AUTOR PRÁCE

SUPERVISOR — **prof. RNDr. Tomáš Šikola, CSc.**
ŠKOLITEL

BRNO 2023

Abstract

The aim of the presented PhD thesis was to develop and analyze gallium nitride (GaN) nanostructures in three different forms. Firstly, three dimensional GaN nanocrystals prepared on graphene were studied from the perspective of the intrinsic crystal properties as well as growth statistics. Adopting the method of droplet epitaxy allowed the formation of such nanostructures at a low substrate temperature ($T \approx 200\,°C$). In order to demonstrate possible applications, the proof of concept of an UV sensitive device was designed and tested with the successful results and the great promise to the future work. Secondly, two dimensional GaN nanostructures were prepared on a pristine silicon surface also at low temperature ($T \approx 200\,°C$). Following experiments were focused on a study of a crystal structure and an elemental analysis as these structures have been observed for the first time. Two dimensional structures are promising candidates into the high power applications which are emerging in these days. Thus, preparation of such 2D GaN nanostructures serves as a solid foundation for the further research. Thirdly, one dimensional GaN horizontal nanowires were fabricated on different sapphire planes. The prepared nanowires provided adequate dataset for the subsequent data analysis related to the growth kinetics. Collected dataset was used for verification of the developed theoretical model of the nanowire growth. It has been shown that the theoretical model describes the growth of nanowires with great precision and, thus, provide a useful insight into the growth mechanisms.

Keywords: GaN, nanocrystals, nanowires, deposition, graphene, sapphire, scanning electron microscopy, atomic force microscopy, Raman spectroscopy

Abstract in Czech

Předkládaná dizertační práce se zabývá výrobou a analýzou gallium nitridových (GaN) nanostruktur ve třech odlišných formách. V prvním případě byl zkoumám trojdimenzionální GaN ve formě nanokrystalů rostených na grafenu. Nanokrystaly byly připraveny s využitím techniky droplet epitaxy, která mimo jiné umožňuje růst nanostruktur za nízké teploty substrátu ($T \approx 200\,°\mathrm{C}$). Studium se zaměřovalo jak na charakterizaci kvality připravených nanokrystalů, tak na statistický popis růstu. V dalším kroku byly připravené struktury využity pro výrobu fotodetektoru citlivého na ultrafialové světlo. Výroba fotodetektoru a jeho úspěšné použití slouží jako základ pro navazující výzkum. Ve druhém případě byly studovány dvoudimenzionální GaN nanostruktury, které byly rovněž připraveny za nízké teploty křemíkového substrátu. Následná analýza se soustředila na popis krystalové struktury a prvkovou analýzu, neboť byly takovéto struktury pozorovány vůbec poprvé. Další rozvoj možností přípravy těchto nanostruktur je předmětem navazujícího výzkumu. Ve třetím případě byly zkoumány jednodimenzionální GaN nanodráty připravené na safírovém substrátu. Účelem tohoto projektu bylo získání datasetu pro ověření teoretického modelu, který popisuje růst horizontálních nanodrátů. Na základě sběru a analýzy dat se podařilo modelovat růstovou dynamiku GaN nanodrátů, která byly v souladu s teoretickým modelem.

Klíčová slova: GaN, nanokrystaly, nanodráty, depozice, grafén, safír, skenovací elektronová mikroskopie, mikroskopie atomárních sil, Ramanova spektroskopie

Contents

1 III-nitride semiconductors

The III-nitride semiconductors represent a group of materials in which representatives of the group-III of the periodic table of elements form chemically stable compounds with nitrogen. Namely, those are boron nitride (BN), aluminium nitride (AlN), gallium nitride (GaN), indium nitride (InN) and thallium nitride (TlN). The III-nitrides are hot candidates for using in modern electronic and photonic devices. The main reason for that is the range of band-gap values for individual compounds as well as tunability of it. Figure 1 (a) shows the band-gaps of binary III-nitride compounds representatives spread over wide energy interval from 7 eV in case of a monolayer of AlN to 0.7 eV in case of a bulk InN [1, 2]. Moreover, tuning of stoichiometric ratio in ternary compounds leads to a continuous change in the wavelength emitted from such a structure as illustrated in Figure 1 (b) [3].

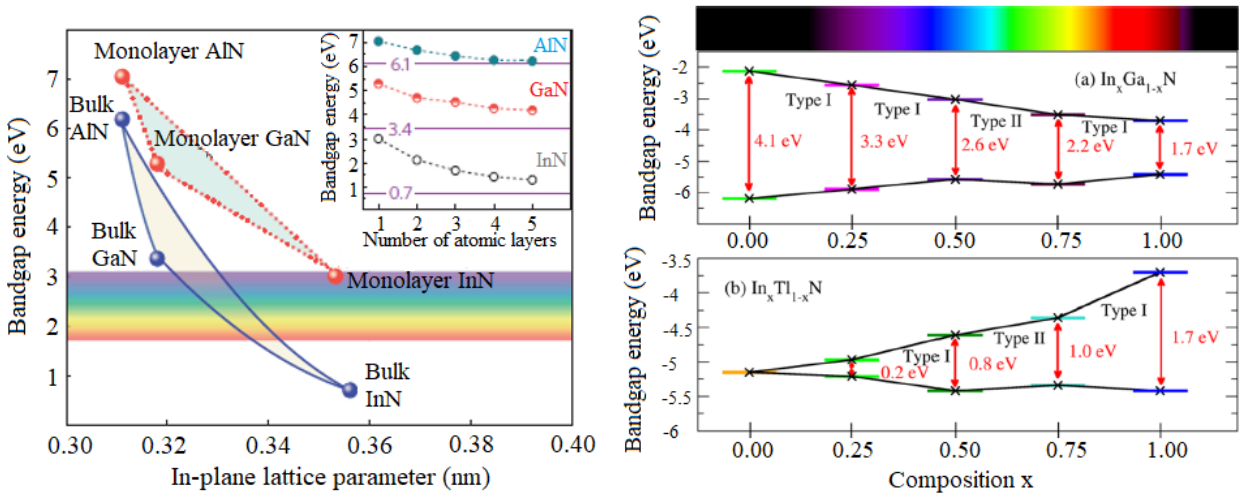

(a) (b)

Figure 1: (a) Band-gap energies of III-nitrides with respect to the electromagnetic spectrum. Band-gap energies of hexagonal III-nitrides with respect to the number of monolayers is plotted in the inserted box [4]. (b) Composition-based tuning of band-gap energies in ternary compounds of $In_xGa_{1-x}N$ and $In_xTl_{1-x}N$ [3].

The suitability of materials for applications is defined by their electrical and optical properties. While a breakdown voltage and a thermal conductivity are relevant aspects for transistor, the materials useful for light emitting devices are sorted mostly based on a band-gap energy. Group III-nitrides provides promising candidates which could meet such requirements out upon these devices as the binary or ternary compounds cover whole spec-

trum from near infra-red represented by InN to deep ultraviolet representedy by AlN. Up to date, there is a number of devices covering infra-red [5, 6, 7], visible light [8, 9, 10] and ultraviolet part of the electromagnetic spectrum [11, 12, 13, 14, 15]. Three technologies based on III-nitrides which impacted the society or appears to be promising parts of advanced devices in the future are shortly described below. Of particular interest - with respect to the focus of the presented PhD thesis - is GaN whose physical properties are summarized in detail in Section 1.4.

1.1 Light-emitting diods

The comparison of efficiency and lifetime of an obsolete tungsten filament light bulb illustrates the impact of LEDs greatly. While the average filament light bulb requires approximately 60 W to produce brightness of 350 lumen (efficiency $6\,\mathrm{lm}\cdot\mathrm{W}^{-1}$), the LED requires only 5 W for the same brightness (efficiency $70\,\mathrm{lm}\cdot\mathrm{W}^{-1}$). In addition, the 2 000 hours lifetime of the incandescent bulb compared to 15 000 hours in case of LEDs reveals the benefits of semiconductors based technology. Such arguments could be easily interpreted in a way that LED lighting saves the energy consumption by far. In fact, recent studies have shown that the LED lighting technology reduced energy consumption only temporarily. As the cost of the LED lighting decreases significantly, the expansion of lighting in households and a public sphere erodes the gains from more efficient technology [16]. Data spanned over three centuries, six continents and five lighting technologies gives a clear conclusion that *"there is a massive potential for growth in the consumption of light if new lighting technologies are developed with higher luminous efficacy and lower cost of light"* [17]. Thus, the real impact of the LED technology is more likely an expansion of lighting rather than saving the energy.

1.2 High power devices

Another benefit resulting from the wide band-gap semiconductors is their suitability for high power applications. The role of the power devices in the future technologies is diverse. From the microturbines designed to output power ranging from 25 kW to 500 kW to energy storage systems design as stand-alone or smart grid subsystems [18]. Nowadays, the most promising candidate for high power applications is silicon carbide (SiC). With the 10 times

higher breakdown voltage ($E_b = 4.9 \times 10^6\,\mathrm{V \cdot cm^{-1}}$) and 3 times higher thermal conductivity ($c_\tau = 3\,\mathrm{W \cdot cm^{-1}}$) in comparison with silicon, the operation temperature can be up to 200 °C [19]. In fact, SiC Schottky diodes already compete with the Si power diodes on the commercial market. Their comparison at working voltage 1 200 V demonstrates a 30 % decrease in total power loss at 150 °C in case of SiC Schottky diode [20].

The comparison of electrical properties of 600 V Si MOSFET, 600 V SiC MOSFET and 600 V GaN HEMT (High electron mobility transistor) at the temperature of 150 °C provided in [21] shows superiority of SiC and GaN over Si. At frequency of 25 kHz and 50 % of duty cycle (a fraction of one period in which the device is active) the energy loss of silicon device was 205 μJ which was more than 10 times higher than in case of SiC (17 μJ) and 20 times higher than in case of GaN device (10 μJ). So the state-of-art silicon technology together with promising III-nitrides' properties give a solid foundation for a following development of high power GaN-Si / SiC-Si devices and this trend will be probably speed up in the near future with new demands on new generation electronics [22].

1.3 Ultraviolet detectors and emitters

Ultraviolet (UV) detectors and emitters are widely used in advanced devices in both military and civil spheres. The ozone layer of the Earth hugely absorbs the radiation in the wavelength interval of 240 - 280 nm. For that reasons, these wavelengths are almost non-existent in the atmosphere. This UV spectral region is thus suitable for observing, for example, electrical discharges as a part of missile-detector systems [23, 24]. Another applications of UV devices could be their implementation into water purification processes [25]. Because of the continuing urbanization the good quality water supply starts to be a serious issue all over the world. The devices producing UV light could be suitable supplement to physical (e.g. filtration) and chemical (e.g. hydrochloride treatment) methods of removing the pollutants from the waste-water [26, 27].

UV detectors can be in general distinguished into two categories - vacuum and solid-state detectors. A detailed review describing photoconductive, Schottky, p-n junction and p-i-n junction - detectors can be found in [23] and [28]. For example, the CVD grown GaN nanowires acting as a photosensitive structure connected to the electrodes made of silver

nanowires exhibit promising photoresponse to UV light from a xenon lamp [29]. Alternatively, an ultra-long (60-80 μm) AlN nanowire bonded at the opposite ends with golden electrodes exhibits clear photoconductivity response to 325 nm light from He-Cd laser [30]. In both cases, III-nitrides structures were grown on Si/SiO_2 substrate but as other experimental works confirm it is also possible to introduce more unconventional substrates as reviewed in [31].

1.4 Physical properties of gallium nitride

Gallium nitride can be found in two stable crystalline forms at ambient conditions - zincblend (cubic) and wurtzite (hexagonal) as shown in Figure 2 (a). While the cubic form is determined by ABCABC stacking sequence of (111) close packed layers, the wurtzite structure is characterized by ABABAB stacking sequence of close packed (0001) planes. Since most of the efforts is placed into the growth of the wurtzite structures, the further description will also focus on this structural form of GaN.

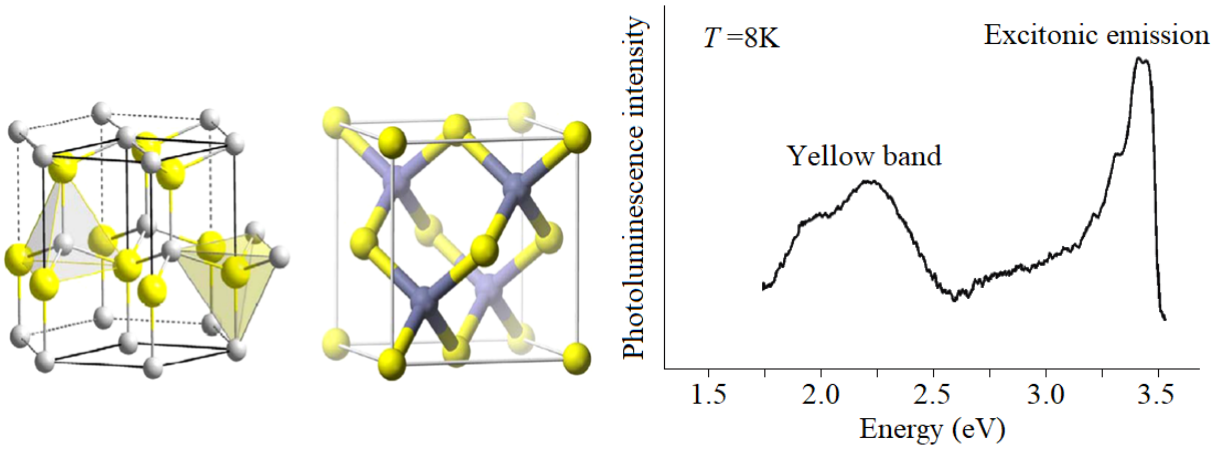

Figure 2: (a) Hexagonal wurtzite and cubic zincblende structures of GaN nitride [32]. (b) Photoluminescence response of GaN to $\lambda = 325\,\text{nm}$ irradiation [33].

GaN is extensively studied for its optical properties. The band gap energy of $E_b = 3.42\,\text{eV}$ at 300 K corresponds with the wavelength of $\lambda = 362\,\text{nm}$. The overview of the band gap energy measurement at various temperatures can be found in [34]. The photoluminescence

spectrum is illustrated in Figure 2 (b) [35, 36].

	E_G (eV)	λ (nm)	a (Å)	E_b ($10^6 \cdot V \cdot cm^{-1}$)	μ_e ($cm^2 \cdot V^{-1} \cdot s^{-1}$)	c_τ ($W \cdot cm^{-1}$)	Ref.
InN	0.64	1900	3.53	0.35	2050	0.8	[37, 38]
Si	1.1	1127	5.43	0.3	1400	1.5	[39]
4H-SiC	3.26	380	3.08	3	900	4.9	[19, 39]
GaN	3.42	362	3.19	5	900	1.3	[38]
AlN	6.14	200	3.11	11	300	2.9	[38]

Table 1: Electrical and optical characteristics of chosen semiconductors (sorted by increasing band gap energy). Energy band gap at room temperature E_G (eV), corresponding wavelength λ (nm), lattice constant a (Å), breakdown voltage E_b ($10^6 \cdot V \cdot cm^{-1}$), electron mobility μ_e ($cm^2 \cdot V^{-1} \cdot s^{-1}$), thermal conductivity c_τ ($W \cdot cm^{-1}$).

The electrical properties of GaN are strongly influenced by intentional, but also unintentional, doping. At the room temperature the electron mobility of GaN reaches $\mu_e = 900\,cm^2 \cdot V^{-1} \cdot s^{-1}$ at a charge carriers concentration of $n = 4 \times 10^{16}\,cm^{-3}$ [38]. At the temperature of liquid nitrogen the electron mobility can reach $\mu_e = 1\,500\,cm^2 \cdot V^{-1} \cdot s^{-1}$ (a charge carrier concentration $n = 8 \times 10^{15}\,cm^{-3}$) [34].

In Table 1, the most prominent binary semiconductors are listed and compared to silicon. As was mentioned above, the different applications put demands on different properties. It can be favourable to combine benefits of several materials in heterostructures.

2 Objectives of presented PhD thesis

Objectives of the presented PhD thesis lay in the experimental work on fabrication and characterization of chosen III-nitrides nanostructures. Specifically, these are three-dimensional gallium nitride (GaN) nanocrystals, two-dimensional GaN nanosheets and one-dimensional GaN nanowires. In all three cases, the nanostructures were prepared using different methods and characterized using different analytic techniques.

The experimental work on three-dimensional GaN nanocrystals is presented in Section 3. GaN nanocrystals were prepared using a droplet epitaxy growth technique in the laboratories of the Institute of Physical Engineering at Brno University of Technology (BUT) under supervision of Prof. Tomas Sikola and Dr. Jindrich Mach. Additional characterization such as SEM imaging, AFM imaging or Raman spectroscopy measurement were done at the Central European Institute of Technology (CEITEC) in Brno. Additionally, the proof of concept of utilizing such nanostructures into UV sensitive device was demonstrated.

An interesting phenomenon of a formation of 2D hexagonal GaN layers at specific conditions was observed during the work on UV sensitive devices. This phenomenon was further studied and the results are presented in the Section 4. Similarly as in the previous case, the experimental part of the work was done at the Institute of Physical Engineering at BUT while the characterization was carried out at CEITEC BUT. The results of this side project were published in [40] and presented by the author as an oral talk at the International Vacuum Conference in Malmö in 2019.

A fourth part of presented thesis, summarized in Section 5, deals with the CVD growth of GaN nanowires and the study of nanowires growth kinetics. The value of this project is in the connection between the theoretical model and its experimental verification. The experimental part of this project was done during an internship in the group of Prof. Ernesto Joselevich in the Weizmann Institute of Science in Israel. The theoretical model was developed by Prof. Vladimir Dubrovskii at St. Petersborough University in Russia. The results of this project were published in *Nanomaterials* [41].

3 GaN nanocrystals on graphene

Silicon wafer (n-type Si(100), $\rho = (0.577 - 0.601)\,\Omega \cdot \mathrm{cm}$, ON Semiconductors) with a 285 nm thick thermally grown silicon dioxide layer was chosen as a substrate for the fabrication of GaN nanocrystals. The thickness of silicone dioxide is especially suitable for graphene-based devices for two reasons. Firstly, this particular thickness is well-known to *"make graphene visible"* even by optical methods because the combination of reflectivity of the SiO_2 layer and graphene results in a possibility of seeing the graphene by naked eye [42]. Secondly, 285 nm thick silicon dioxide layer is sufficient enough to act as an insulating layer which allows the measurement in a FET arrangement.

As the first step, the distribution of gallium islands on graphene laying on silicon substrate was studied. The time of the deposition of gallium was set to 50 minutes. During that period of time, 4.3×10^{16} atoms per cm^2 impacted the surface which is equivalent to 10 monolayers. The effect of the substrate temperature on the distribution and size of gallium islands formed on graphene can be seen in Figure 3.

Figure 3 (a) - (e) shows the evolution of gallium droplets in a temperature window from 150°C to 350°C. There are two types of islands - bright islands and dark islands. Figure 3 (f) shows an AFM profile of the islands grown at 350°C. In this AFM image, the difference between the bright and dark islands is clearly visible. While the bright islands are more hemispherical, the dark islands appear to have flat tops.

Once the graphene was covered with gallium droplets, the second phase of the growth process - nitridation - was initiated. The three sequences of gallium deposition and subsequent nitridation resulted in formation of GaN nanocrystals. The size of formed nanocrystals is heavily dependent on the substrate temperature as can be seen in Figure 4. The size of the GaN nanocrystals grown at a temperature of 240°C (Figure 4 (a)) is in the range of (20 - 30) nm. As the temperature of the substrate is rising the GaN crystals grow in size which can be up to 100 nm at 280°C and higher.

Despite the fact that the quality of nanocrystals seems to be sufficiently high, the quality of the graphene layer suffers by the atoms/ions irradiation. Figure 5 (a) shows the Raman

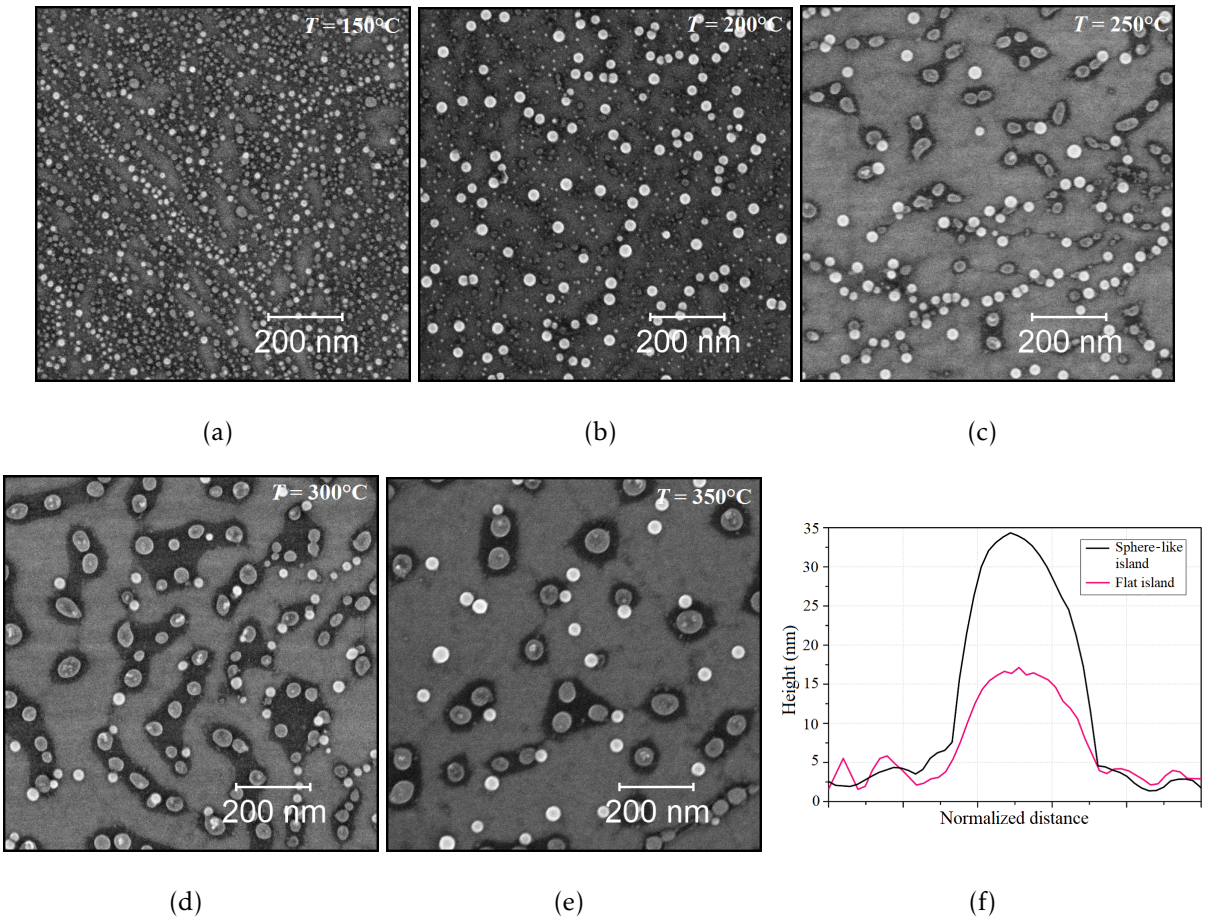

Figure 3: SEM images of formed gallium islands on graphene at (a) 150°C, (b) 200°C, (c) 250°C, (d) 300°C and (e) 350°C. (f) AFM profile of gallium islands on grapehene at 350°C. The diameters of islands were normalized in order to show the difference in height. The SEM images were taken by a FEI Verios 460L microscope at a landing energy of $E = 8\,\text{keV}$ and a probe current of $I = 25\,\text{pA}$. AFM images were taken by an ICON Brucker microscope using the ScanAssyst mode and probe.

spectra of a graphene layer after one (green line), two (blue line) and three (red line) sequences. In all three cases, the absence of zhe 2D peak and presence of the D peak brings a sufficient evidence that graphene layer quality is affected is significantly affected and goes down with the number of sequences. In our experimental arrangement, the resistance of a graphene monolayer placed on SiO_2 was typically around $900\,\Omega$. The formation of nanocrystals on graphene (graphene exposed to Ga atoms and nitrogen ions) increased the resistance up to $15\,000\,\Omega$ which was a significant obstacle for the measurement of electrical properties.

The photoluminescence response of GaN nanocrystals on a UV excitation laser (λ =

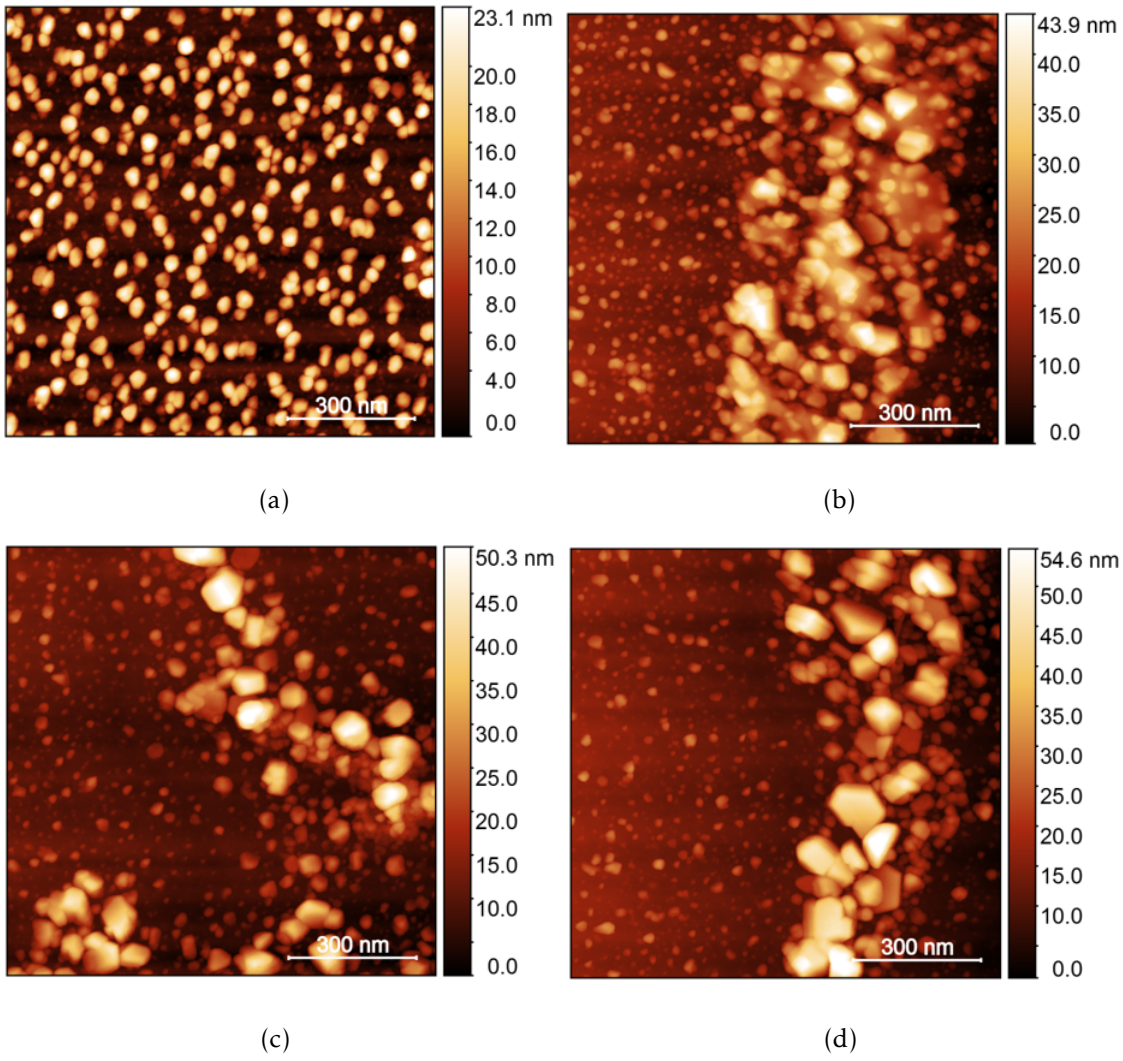

Figure 4: AFM images of nanocrystals formed on graphene at (a) 240°C, (b) 260°C, (c) 280°C and (d) 300°C. AFM images were taken by an ICON Brucker microscope using the ScanAssyst mode and probe.

352 nm) is plotted in Figure 6. The comparison of GaN nanocrystals grown using different nitrogen ion energy reveals several aspects. The blue emission peak corresponding with the inner electron transition is located at 3.33, 3.41 and 3.42 eV for ions energy 50, 40 and 30 eV, respectively.

The above mentioned results are in a good agreement with the former experimental work of our group [43] as well as with the theoretical description of GaN nanocrystals formation provided in [44]. The formation of GaN nanocrystals is a result of interactions of nitrogen ions with the gallium atoms from the gallium droplet. The crystallization starts at the solid-liquid interface, i.e. in the close proximity of liquefied Ga droplet and a solid sub-

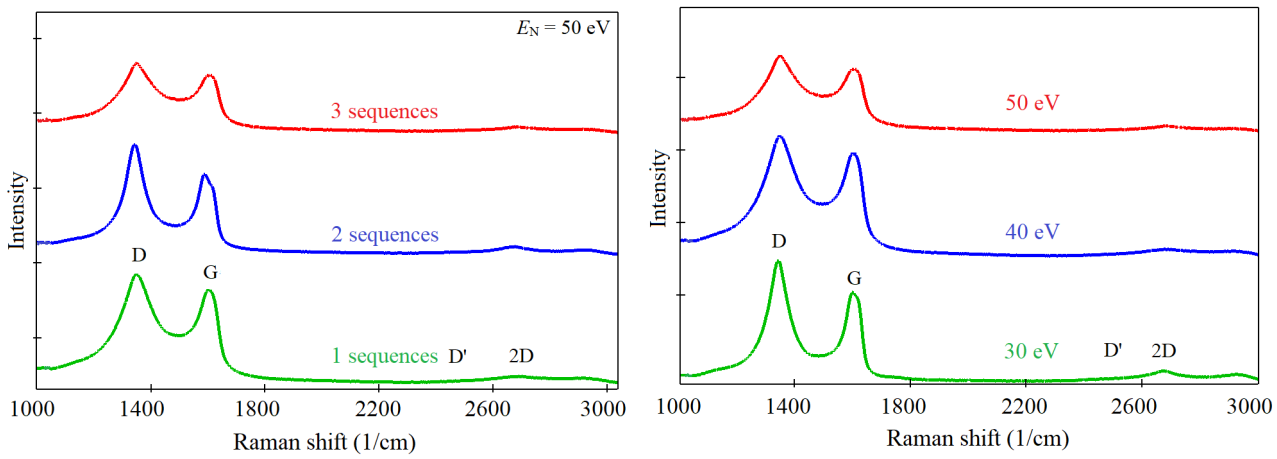

(a) (b)

Figure 5: (a) Raman spectra corresponding to the grown GaN on graphene using different number of deposition sequences. (b) Raman spectra of graphene illustrating the effect of used nitrogen ions energy on the quality of graphene layer. The Raman spectra were measured by a Witec Raman system using lambda = 532 nm excitation laser.

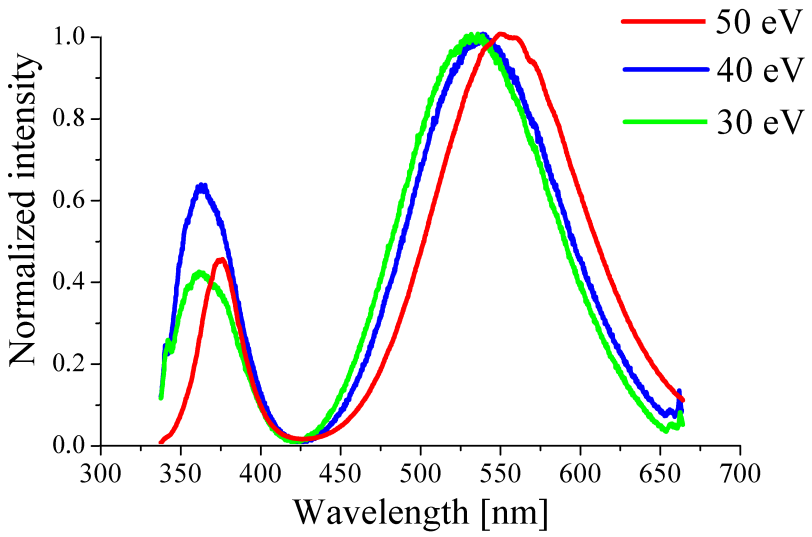

Figure 6: Photoluminiscence spectra of GaN nanocrystals grown at different energies. The spectra were taken by an NT-MDT Ntegra Spectra Raman system using 352 nm laser.

strate surface interface. There are several paths through which nitrogen ions can diffuse to this region - (i) entering the gallium droplet and diffusing through the liquefied volume, (ii) diffusing along the droplet surface or (iii) diffusing over the substrate surface as described by Gerlach [44].

3.1 Fabrication of an UV sensitive photodetector

Fabrication and characterization of GaN nanocrystals grown on graphene opened a way for the implementation these nanostructures into a functional device. Motivation behind this application is combining two research directions in our group - GaN nanocrystals and graphene.

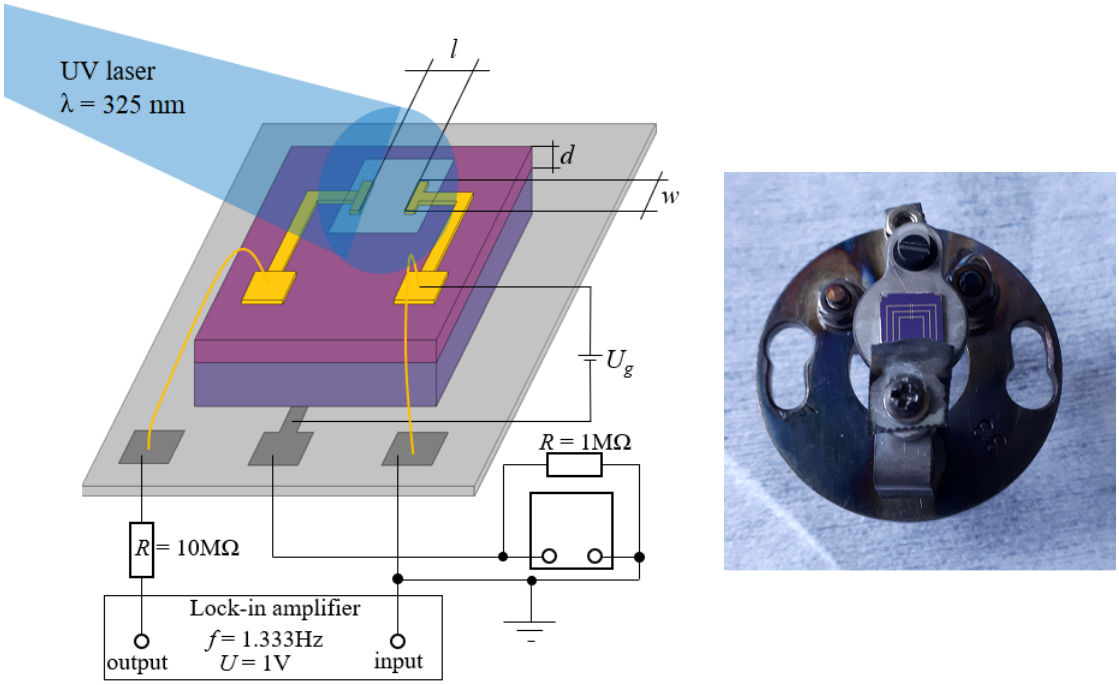

(a) (b)

Figure 7: (a) Schematics of an experimental setup for detection of the response to the UV light with schematics of the electrical connection. (b) Photo of the UV photodetector attached to a sample holder with a PBN plate.

Figure 7 (a) shows a schematic representation of the UV sensitive device design. The silicon with a 280 nm thick silicon dioxide layer is used as a substrate. There are two electrodes on the substrate surface made of gold which are separated by a 100 μm gap. The area of the gap is covered with a graphene sheet in such a way that the graphene is in an ohmic contact with both electrodes. The graphene sheet is covered with the gallium nitride nanocrystals which behave as UV sensitive structures. Prepared silicon samples with fabricated electrodes and graphene loaded onto the sample holders with PBN heating plate are shown in Figure 7 (b). The prepared sample attached onto ceramic expander is placed in front of an

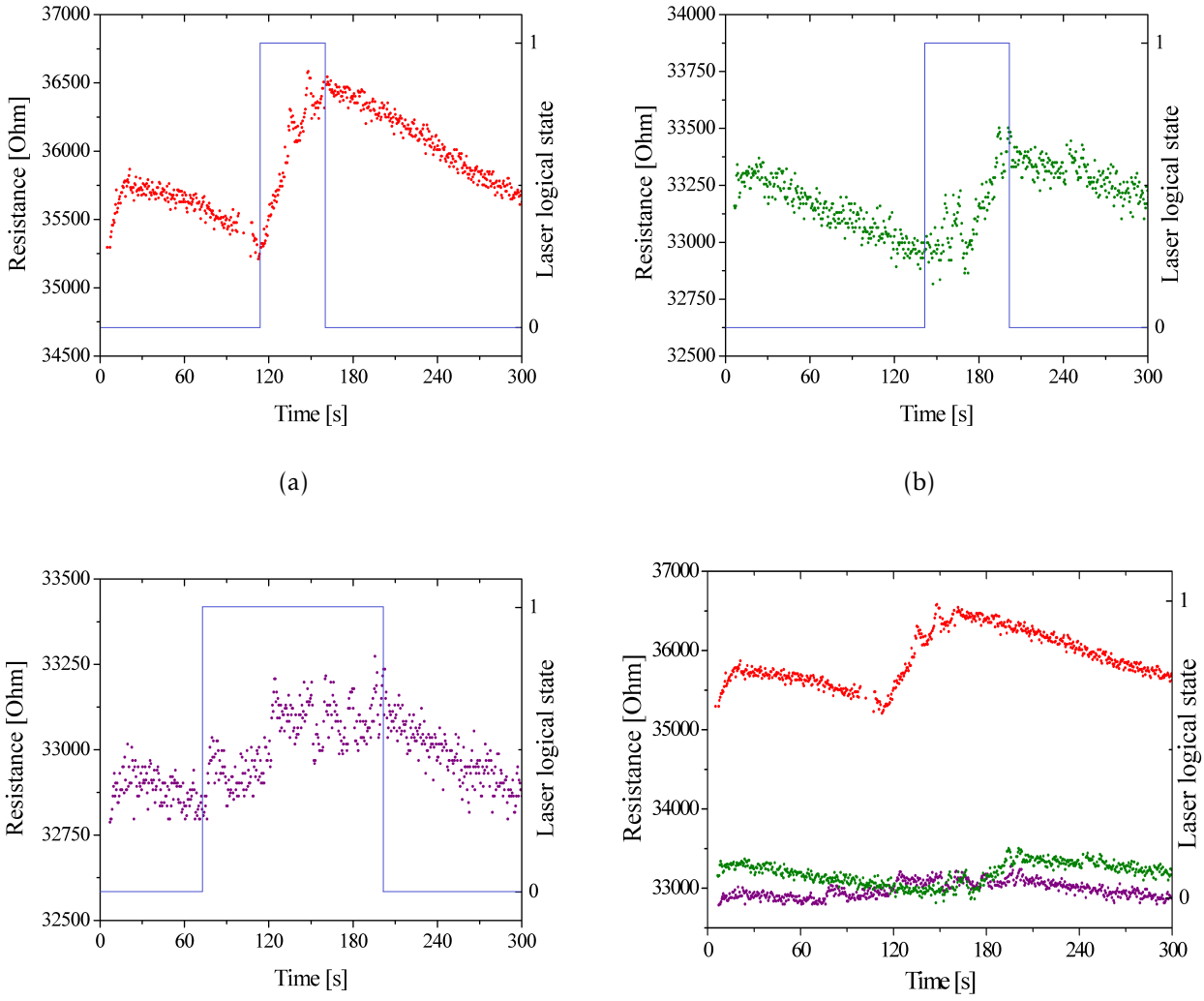

Figure 8: Response of the fabricated UV sensitive device to a UV light irradiation in the case of graphene covered with GaN nanocrystals (green line) and without them (red line).

UV laser. The He-Cd laser produces monochromatic UV light of wavelength 325 nm. A mechanical shutter located at the far end of the laser instrument provides an easy way of selecting on/off operation state. The sample electrodes are connected to a Keithley/Lock-in measurement system developed in our group via silver contacts of the ceramic expander [45]. The voltage 1 V at a frequency of 1.333 kHz is set as an output signal of a SR830 Lock-in amplifier (Stanford Research Systems). A signal goes to the first electrode on the sample through a 10 MΩ resistor. The second electrode is then connected with the ground potential. The current flowing through the graphene is then measured using a LabView software developed in our group. In addition to the basic circuit, the Keithley source provides gate

voltage and thus allows measuring in a FET-like arrangement.

In the following experiments, the sample was irradiated with the UV laser for varying time interval. Figure 8 shows the measured response of the sample irradiated for (a) 40 s, (b) 60 s and (c) 120 s. In all cases, the instant change in resistance correlates with switching the laser on and off. In the first measurement, the rapid increase of resistance by 1 000 Ω is observed. In the second measurement, the resistance increases roughly by 500 Ω. The change in resistance in the third measurement is less dramatic when it increases by only 300 Ω despite the fact, that the irradiation lasted for 120 s.

Figure 8 (d) reveals a direct comparison of these measurement on one sample. It can be clearly seen that the initial resistance decreases with each consecutive photodetector irradiation. From approximately 36 kΩ for the first measurement to 33 kΩ for the last measurement. However, this drop in resistance is still only 9% change from the initial value. Additionally, the amplitude of the response is also decreasing withthe irradiation intervals. This could be attribute to a decrease in quality of either the graphene layer or gallium nitride crystals.

4 Two dimensional GaN

The growth of the hexagonal GaN was carried out in a UHV complex system in the laboratory of Institute of Physical Engineering at BUT. The process started with the substrate pretreatment which ensured the cleanliness of the surface. Then, a two-step growth process took place divided into (i) a deposition of gallium and (ii) a post-nitridation with low energy ions ($E = 50\,\mathrm{eV}$).

The preparation of n-type doped silicon Si(111) with 4° and 0.2° miscut (resistivity $\rho = (0.029 - 0.030)\Omega \cdot \mathrm{cm}$) followed the routine of sonication in different chemical substances, degaussing at a temperature of $T = 700\,°\mathrm{C}$ for 15 hours and flash-annealing routine with a peak temperature of $T = 1250\,°\mathrm{C}$ for 12 cycles. A miscut angle defines the size of terraces formed at the silicon surface. In this case, a miscut angle of 0.2° provides larger terraces in the range of tens to hundreds nanometers while a miscut angle of 4° provides terraces in the range of tens of nanometers.

Once the preparation was finished, the substrate temperature was set to approximately $T = 300\,°\mathrm{C}$ and the deposition of gallium was initiated. The gallium effusion cell was handled to provided stable flux of gallium atoms of $f = 4{\times}10^{16}\,\mathrm{cm}^{-2} \cdot \mathrm{h}^{-1}$. Deposition of gallium for 1 hour resulted in a formation of the droplets with an average diameter of 50 nm. The density of gallium droplets was approximately 3×10^8 droplets per centimetre squared.

After deposition of gallium, the post-nitridation was conducted for 2 hours. Figure 9 illustrates the effect of a temperature on the nanostructures formed during fabrication process. The effect of temperature was similar for booth types of substrate - Si(111) with 4° as well as 0.2° miscut. At a temperature of $T = 160\,°\mathrm{C}$ (a) the droplets of GaN can be observed. As the temperature rises ($T = 180\,°\mathrm{C}$ (b)), the droplets begin to be deformed and a crystalline part of the GaN protrudes into the direction of incoming nitrogen flux. If the temperature is set to $T = 200\,°\mathrm{C}$ (c), the GaN in the form of triangle-like nanostructure is formed. Once the temperature is increased above $T = 220\,°\mathrm{C}$ (d), the surface is covered by a mixture of triangle-like nanostructures and bulky chunks. The thickness of triangle-like nanostructures varies from 4 nm to 11 nm with the peak maximum at 7 nm.

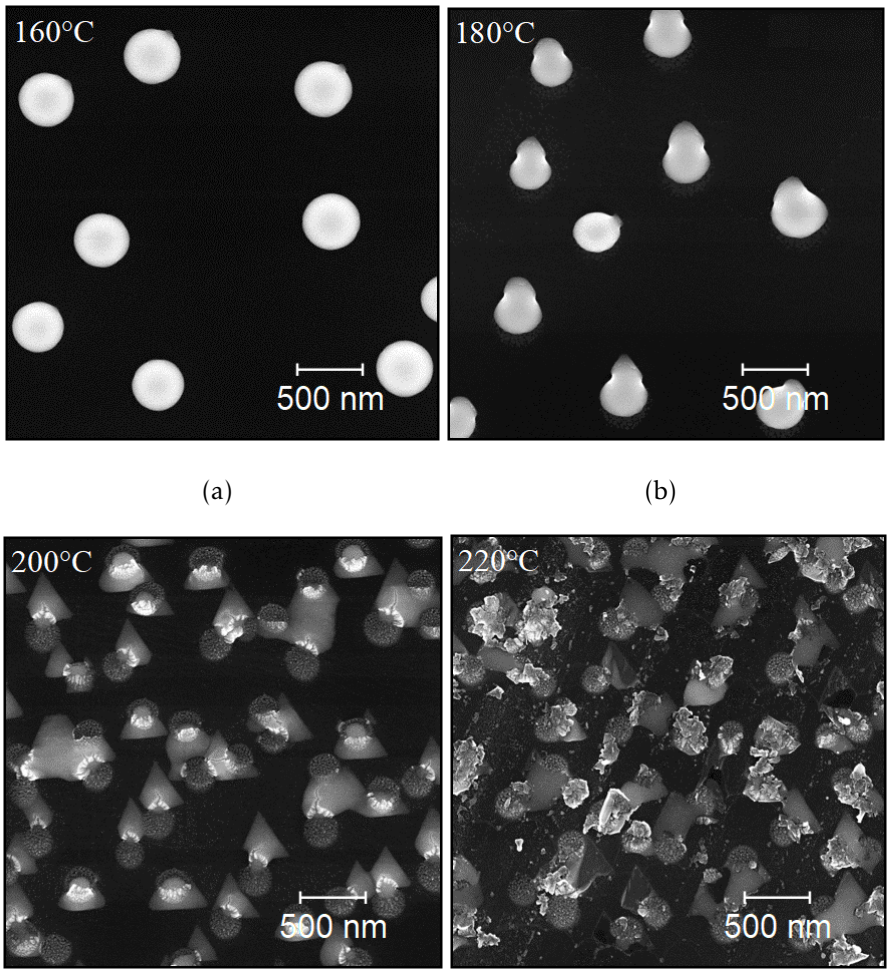

Figure 9: SEM images of GaN grown on pristine Si (111) illustrate the effect of the substrate temperature during post-nitridation. The deposition of gallium was carried out at the temperature $T = 290\,°C$ for 1 hour. The subsequent post-nitridation was carried out for 2 hours at temperatures of (a) $T = 180\,°C$, (b) $T = 200\,°C$, (c) $T = 220\,°C$ and (d) $T = 240\,°C$. The yellow arrow indicates the direction of incoming ions. The SEM images were taken in a FEI Verios 460L microscope at landing energy of 8 kV and probe current of 25 pA.

In order to elucidate the crystalline structure of triangle-like structures, a cross-sectional TEM lamella allowing the STEM imaging was prepared. Figure 10 reveals the cross-section of prepared nanostructure. At first sign, a sharp interface between silicon substrate and formed nanoobject can be seen. The prepared nanostructures consists of original metallic gallium droplet and the crystalline GaN as described in the STEM image.

The zoom-in part of the image shows several layers of silicon Si (111) substrate and crys-

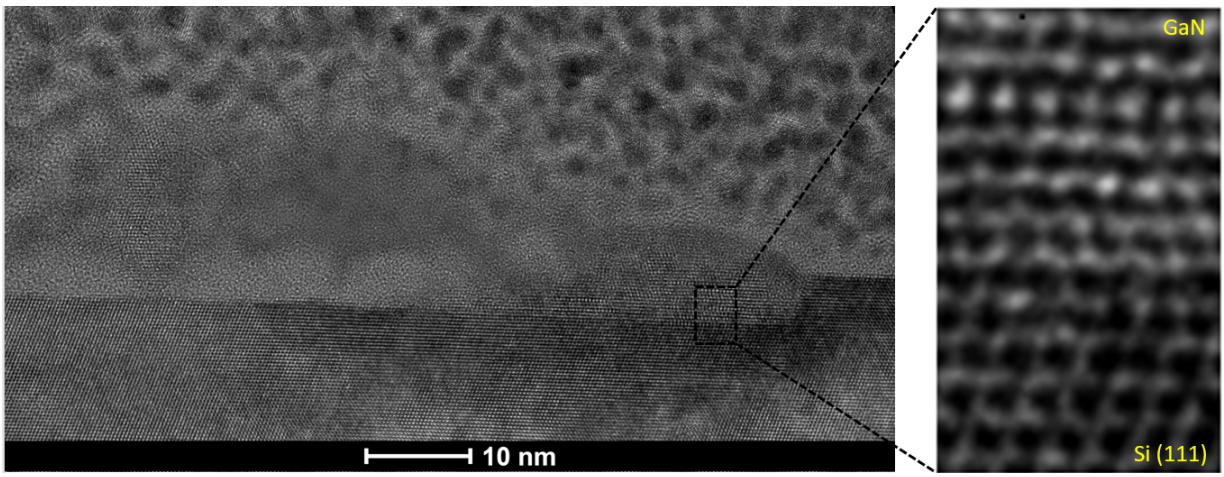

Figure 10: STEM image of the cross-sectional TEM lamella of an amorphous gallium droplet and crystalline GaN on a Si(111) substrate. The zoom-in STEM image of the Si(111) and hexagonal GaN interface.

talline GaN in the close proximity of their interface. The measured interlayer distance of crystalline GaN was 3.14 Å. This value is higher than 2.59 Å observed in wurtzite bulk GaN [46, 47]. The interlayer distance of hexagonal two-dimensional GaN calculated by various numerical approaches varies from 2.22 Å [48] to 3.1 Å [49, 50, 51].

The measured average lattice parameter $a = 3.28$ Å is slightly higher than in a case of wurtzite GaN (3.18 Å) [46, 47, 52] but it is in a good agreement with the calculated value for hexagonal two-dimensional GaN [53] as well. These findings support our hypothesis that the observed triangle-like features could be two-dimensional hexagonal gallium nitride.

In contrary to SEM imaging, an XPS analysis was carried out in situ, i.e. directly after the deposition of gallium and post-nitridation inside the vacuum chamber without exposing the sample to the ambient atmosphere. In situ XPS was performed using an experimental setup consisting of an X-ray source - DAR400 and a hemispherical electrostatic analyzer - EA125 (both Omicron). The experiments were performed at the room temperature using Al Kα radiation. The Figure 11 (a) shows the gallium $Ga2p_{2/3}$ peak in XPS spectrum corresponding to the Ga - N bond in a bulk GaN which serves here as a reference. The peaks in Figure 11 (b) and Figure 11 (c) show different stages of the formation of two dimensional GaN. The peaks in Figure 11 (b) shows the middle phase of the formation process. There are two separate subpeaks in the spectrum corresponding to Ga - N and Ga - Ga types of

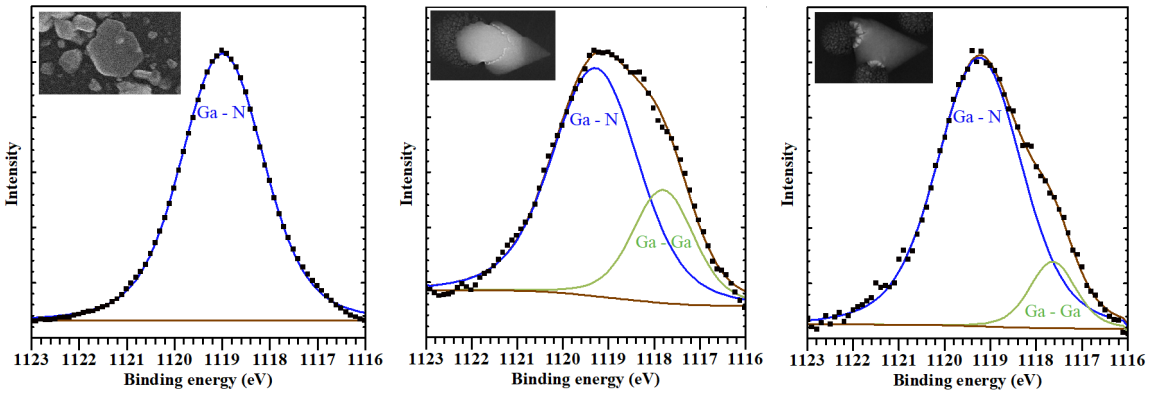

(a) (b) (c)

Figure 11: XPS spectra of gallium $Ga2p_{2/3}$ peak. (a) $Ga2p_{2/3}$ peak corresponding to the bulky GaN used as a reference. (b) $Ga2p_{2/3}$ peak in the middle of the formation of the 2D GaN. (c) $Ga2p_{2/3}$ peak after the formation of the 2D GaN is finished. The subpeak at 1 117.5 eV (green line) is attributed to the metallic gallium while the peak at 1 119.5 eV (blue line) correspond with the Ga - N bond.

bonds. The peak at 1 117.5 eV (green line) corresponds to metallic gallium while the peak at 1 119.5 eV (blue line) correspond toe Ga - N bond in a bulk GaN. Figure 11 (c) reveals the $Ga2p_{2/3}$ peak after the formation of GaN is finished. The Ga - N subpeak became prominent at the expense of the Ga - Ga subpeak which, however, is still present in the spectrum.

With this knowledge the growth mechanism can be outlined. The deposition of gallium results in a formation of metallic gallium droplets spread all over the surface. Once the nitrogen ions start to impinge on gallium droplets, they interact with gallium atoms, and thus post/nitridation is initiated. Several mechanisms enter the reaction as was explained in Section **??** in detail. The metallic gallium is continuously consumed and transformed into hexagonal GaN. The question whether the growth of the triangle-like nanostructures is layer by layer or it is rather initiated in the vicinity of the original droplet and then continue growing in the upstream direction of incoming nitrogen ions is still open. The same stands for the etching of silicon. It is difficult to answer whether this etching is initiated during the deposition of gallium or after the initiation of post-nitridation. The in-SEM growth could possibly reveal the growth mechanisms in the future.

5 GaN nanowires on sapphire

Growth of nanowires is an anisotropic thermodynamically driven process resulting in a formation of one-dimensional nanostructures. As such, the growth can be theoretically described involving several thermodynamic aspects which will be expressed further in this Section. Despite the fact that the nanowires can be grown by various method, the following derivation of a kinetic model is limited to the vapor-liquid-solid (VLS) growth mechanism. The kinetic model of the growth of horizontal nanowires was developed by prof. Dubrovskii based on the mathematical description of mutual interplay between two surface effects - a Gibbs-Thomson effect and a surface diffusion induced growth. The kinetics model was based on the already published kinetic model for the growth of vertical nanowires developed by prof. Dubrovskii as well [54].

There are four possible pathways which ensure the material transport (in this case gallium and nitrogen) into the catalyst (i) diffusion over the surface directly to the catalyst droplet, (ii) diffusion over the surface to the nanowire sidewall and subsequent diffusion along the sidewall, (iii) direct penetration from the flux of incoming source materials to the catalyst droplet and (iv) direct impingement on the nanowire sidewall and subsequent diffusion along the sidewall. Considering all possible pathways the growth rate dL/dt can be formulated as

$$\frac{\mathrm{d}L}{\mathrm{d}t} = 2\Omega I \left\{ 1 - \Theta_{\mathrm{lv}} \mathrm{e}^{\mathrm{R_{GT}/R}} + \left(1 - \Theta_{\mathrm{ls}} \mathrm{e}^{\mathrm{R_{GT}/R}}\right) \left(\frac{\lambda}{\mathrm{R}}\right)^{\mathrm{m}} \right\}, \tag{1}$$

where Ω is the elementary volume, I is the flux rate of the element limiting the growth rate (Ga in this case), $\Theta_{\mathrm{lv}} = n_{\mathrm{l}}^{\infty} = I\tau_{\mathrm{l}}$ is the liquid to vapour activity, $\Theta_{\mathrm{ls}} = n_{\mathrm{l}}^{\infty} = I\tau_{\mathrm{s}}$ is the liquid to solid activity, R_{GT} is the Gibbs-Thomson radius, λ is the diffusion length and m is the power exponent. The liquid to vapour Θ_{lv} and liquid to solid Θ_{ls} activities correspond to the overall diffusion flux of adatoms diffusing either towards or away from the catalyst droplet from vapour or over the surface, respectively. Interestingly, in the limit case of omitted surface diffusion $\lambda \to 0$, Equation 15 is reduced to the length-radius dependence.

5.1 Data collection and fitting

The samples - annealed M-plane and R-plane - were used with a catalyst pattern, i.e. array of $30 \times 5\,\mu m^2$ rectangles array of 5 Å of nickel. The optimal parameters found for the synthesis of GaN horizontal nanowires are summarized in Table 3.

	T_{furnace} (°C)	$T_{Ga_2O_3}$ (°C)	H_2 (sccm)	NH_3 (sccm)	p (mbar)
AM-plane	940	1000	95	3.2	400
R-plane	940	1000	90	2.7	400

Table 2: Optimal parameters for the synthesis of GaN nanowires in CVD reactor using gallium oxide powder.

As can be seen in Figure 12 the nanowires grow on both substrates. However, the quality of guided growth is depending on the surface termination. In a case of the annealed M-plane Figure 12 (a), GaN nanowires are guided by nanogrooves in the main crystallography direction. Nanowires vary in lengths and diameters as will be shown later, but the longest nanowires reach tens of microns. As can be seen in Figure 12 (b), the tip of nanowire is formed with a catalyst droplet. The R-plane surface is also covered with the nanowires as can be seen in Figure 12 (c). However, the epitaxial growth is directed by the crystalography of the surface in this case. Therefore, some of nanowires can grow in the direction not parallel to the main crystallography direction. It is also worth mentioning that the very tip of each nanowire is formed with the droplet catalyst. No self-catalyzed nanowires were observed which suggests that the growth process is initiated by the catalyst.

The diameter of nanowire and corresponding length were measured for each individual nanowire. Measured dataset is plotted in the Figure 13 (a) and (b). However, for further analysis, the radius of the nanowires was plotted as a function of the growth rate. Growth rate was calculated as a nanowire length divided by overall time of synthesis which was 25 min.

Figure 13 (a) represents dataset of nanowires dimensions measured on AM-plane. The radius varies between 10 nm and 25 nm which corresponds with the measured width of the nanogrooves as approximately 40 nm. In contrary, the radius of nanowires grown on R-

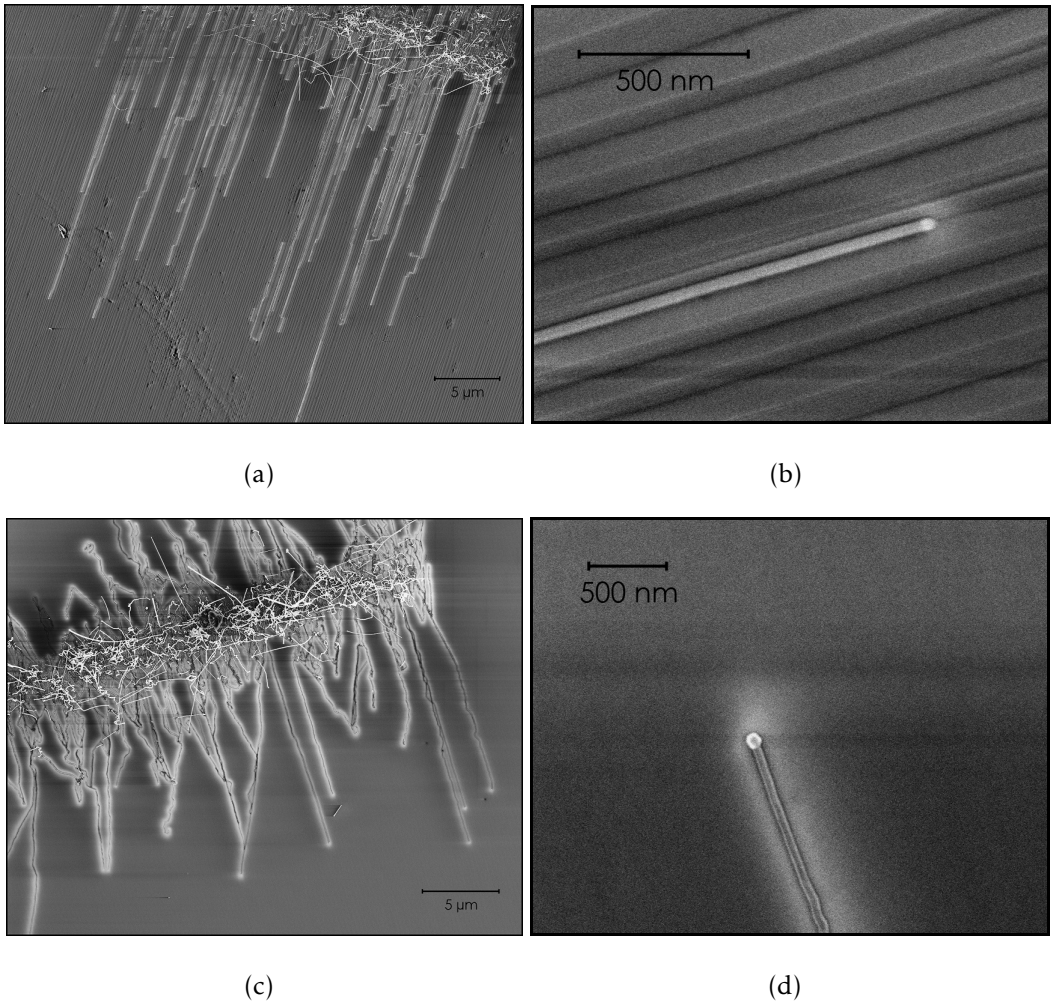

Figure 12: (a, b) GaN guided horizontal nanowires on the annealed M-plane. (c, d) GaN horizontal nanowires on the R-plane.

plane varies from 20 nm to 50 nm as can be seen in Figure 13 (b). The maximal measured length was approximately 30 μm which corresponds (considering the 25 min as a time of the synthesis) to the growth rate of $1.4\,\mu\mathrm{m}\cdot\mathrm{min}^{-1}$ as can be seen in the both plots.

Selected data (Figure 13 (c) and Figure 13 (d)) were then fitted using Equation 15. Obtained parameters are summarized in Table 3. The power factor m was found to be close to 2 for both the AM-plane ($m_{\mathrm{AM}} = 2.02$) and the R-plane ($m_{\mathrm{R}} = 1.93$). As was described above the power factor $m = 2$ is associated with the surface diffusion of adatoms towards the catalyst droplet. Hence, the diffusion along the sidewall is limited in this case. The diffusion length λ differs from ≈ 41 nm for the AM-plane to ≈ 47 nm for the R-plane. The diffusion length in both cases is substantially smaller than the overall lengths of nanowires which

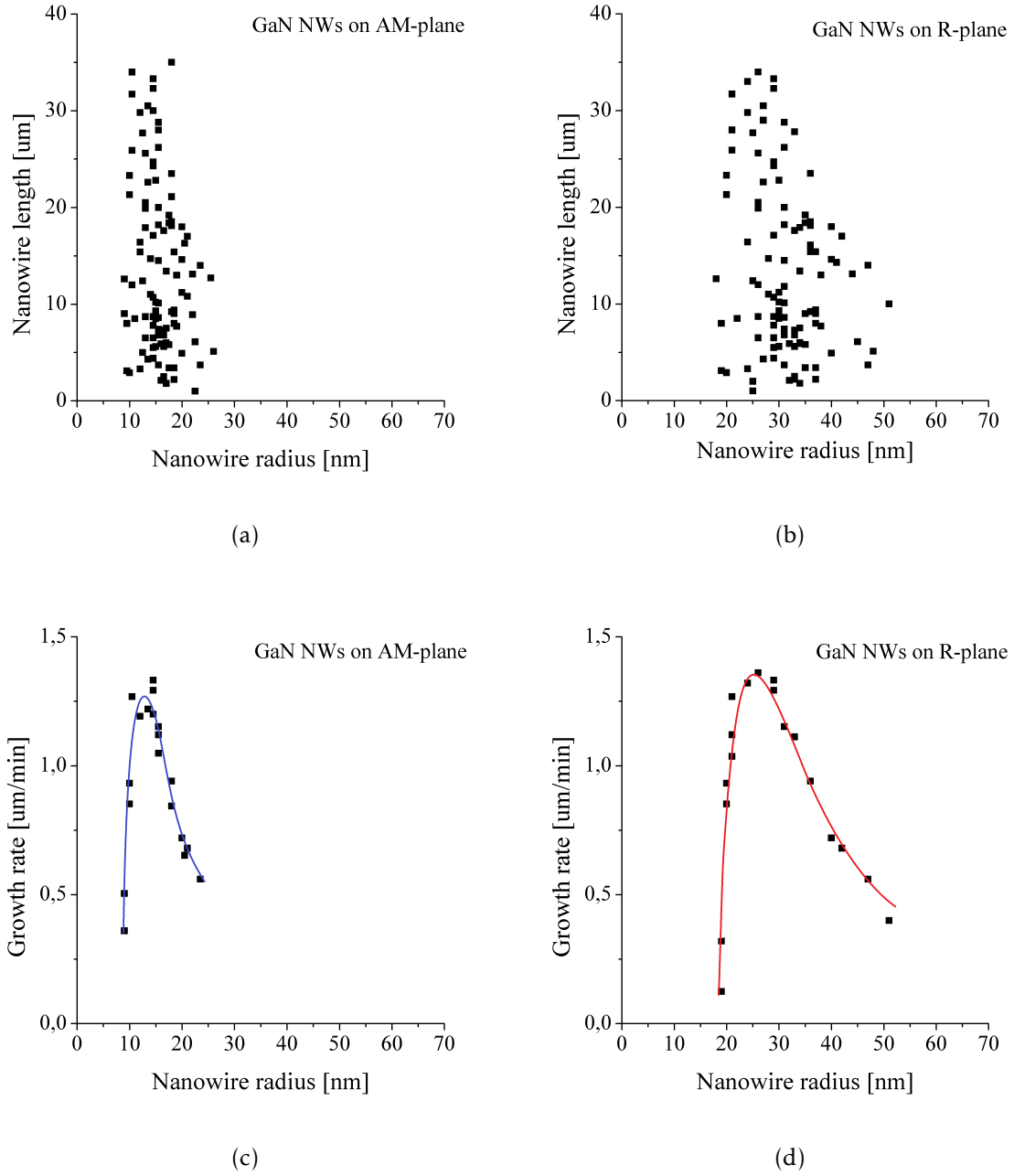

Figure 13: Dependence of nanowire length with respect to nanowire radius of GaN nanowires grown on (a) AM-plane and (b) R-plane. Envelope data of GaN nanowires grown on (c) AM-plane and (d) R-plane fitted with the kinetic Equation 15. The y-axis is recalculated from the length to the grow rate (L/t, where t is the time of synthesis).

varies from 5 μm to as much as 30 μm. Interestingly, the diffusion length on the AM-plane is comparable to the width of the surface nanogrooves. In the same time, it is 13 % smaller in comparison with the R-plane with a flat surface. This can explain the difference in maximum diameter of nanowires which is almost two times bigger on the R-plane compared to

Sap. plane	$\Omega I\,(\mu\mathrm{m}\cdot\mathrm{min}^{-1})$	Θ_{lv}	Θ_{ls}	$R_{\mathrm{GT}}\,(\mathrm{nm})$	$\lambda\,(\mathrm{nm})$	m
AM-plane	0.63 ± 0.12	1.00 ± 0.05	0.47 ± 0.03	6.02 ± 0.13	40.93 ± 2.71	2.02 ± 0.15
R-plane	5.67 ± 0.78	1.00 ± 0.05	0.69 ± 0.02	5.34 ± 0.09	46.85 ± 0.55	1.93 ± 0.17

Table 3: Fitting parameters used and calculated based on the kinetic model.

the AM-plane. Since the nanogrooves act as a natural barrier for the adatoms diffusion, the amount of the source material capable of diffusing into the catalyst droplets is effectively reduced which results in a smaller maximum diameters while the length is comparable on both sapphire planes.

The deduced power exponents m close to 2 are in good agreement with the already reported values for flat (sapphire C-plane) $m = 1.8 \pm 0.2$ and faceted (sapphire AM-plane) $m = 1.8 \pm 0.1$ Au-catalyzed ZnS and ZnSe horizontal nanowires [55]. As ZnS and ZnSe are representatives of II-VI semiconductors while the GaN is representative of III-V group, the obtained result may be generalized to surface guide horizontal nanowires. The mechanisms of the growth of horizontal nanowires is preferentially mediated by two-dimensional diffusion of adatoms over the substrate surface directly towards the catalyst droplets. This mechanism differs from the situation in the case of vertical nanowires, whose growth is dominated by the one-dimensional diffusion along the nanowire sidewalls[56].

6 Conclusion

I have presented results of three individual projects which have been done during my PhD program. All projects were related to a fabrication and characterization of III-V group representative - GaN. I have presented preparation of GaN in three different forms - 1D, 2D and 3D structures - using different fabrication techniques.

First, 3D GaN in the form of nanocrystals prepared using droplet epitaxy method has been demonstrated. The fabricated GaN nanocrystals were studied using different analytical techniques in order to elucidate the quantitative aspect of the growth as well as the quality of prepared structures. GaN nanocrystals were grown on a graphene layer which have brought a possibility to fabricate an UV sensitive photodetector. A proof of concept - a design and basic functionality - has been explored with a positive outcome which paves the way for following research. As a result, a new PhD position focusing on further exploration of the designed UV sensitive photodetector has been opened in our group.

Second, growth of 2D GaN at low temperatures has been studied. 2D GaN nanostructures were grown on two different Si substrates and analyzed by various techniques such as XPS, TEM and Auger spectroscopy to provided qualitative study of their nature. The mechanisms of their growth was suggested based on the provided measurements and already published literature. The results of this side project were published in *Nanoscale Advances* [40] and presented as an oral talk at the International Vacuum Conference in Malmo in 2019.

Third, study of a 1D GaN nanowires growth kinetics has been performed. This project consisted of fabrication of GaN nanowires on various sapphire substrates and following measurement of their dimensions. Collected data were used for evaluation of a proposed theoretical model of the horizontal GaN nanowires growth. This effort is a part of a long-term cooperation between the group of Prof. Ernesto Joselevich in the Wiezmann Institute of Science and Prof. Vladimir Dubrovskii from St. Petersborough University in Russia. The results were published in *Nanomaterials* [41]. Provided data on GaN nanowires supported the model and extend its applicability to a III-V group of semiconductors.

References

[1] J. Wu and W. Walukiewicz. Band gaps of InN and group III nitride alloys. *Superlattices and Microstructures*, 34(1-2):63–75, 2003.

[2] J. Wu, W. Walukiewicz, W. Shan, K. M. Yu, J. W. Ager, S. X. Li, E. E. Haller, H. Lu, and W. J. Schaff. Temperature dependence of the fundamental band gap of InN. *Journal of Applied Physics*, 94(7):4457–4460, 2003.

[3] M. S. Prete, A. Mosca Conte, P. Gori, F. Bechstedt, and O. Pulci. Tunable electronic properties of two-dimensional nitrides for light harvesting heterostructures. *Applied Physics Letters*, 110(1):012103, 2017.

[4] Z. Y. Al Balushi, K. Wang, R. K. Ghosh, R. l. A. Vila, S. M. Eichfeld, J. D. Caldwell, X. Qin, Y. Lin, P. l. A. DeSario, G. Stone, et al. Two-dimensional gallium nitride realized via graphene encapsulation. *Nature materials*, 15(11):1166, 2016.

[5] Junqiao Wu. When group-III nitrides go infrared: New properties and perspectives. *Journal of Applied Physics*, 106(1):5, 2009.

[6] D. Z. Ting, A. Soibel, A. Khoshakhlagh, S. A. Keo, B. Rafol, A. M. Fisher, B. J. Pepper, E. M. Luong, C. J. Hill, and S. D. Gunapala. Advances in III-V semiconductor infrared absorbers and detectors. *Infrared Physics & Technology*, 97:210–216, 2019.

[7] A. Ajay, Y. Kotsar, and E. Monroy. Infrared emitters using III-nitride semiconductors. In *Nitride Semiconductor Light-Emitting Diodes (LEDs)*, pages 587–617. Elsevier, 2018.

[8] Shuji Nakamura. Nobel lecture: Background story of the invention of efficient blue InGaN light emitting diodes. *Reviews of Modern Physics*, 87(4):1139, 2015.

[9] H. P. Maruska and W. C. Rhines. A modern perspective on the history of semiconductor nitride blue light sources. *Solid-State Electronics*, 111:32–41, 2015.

[10] Isamu Akasaki. Nobel lecture: Fascinated journeys into blue light. *Reviews of Modern Physics*, 87(4):1119, 2015.

[11] Y. Li, M. Dvorak, P. N. Nesterenko, N. Nuchtavorn, and M. Macka. High power deep UV-LEDs for analytical optical instrumentation. *Sensors and Actuators B: Chemical*, 255:1238–1243, 2018.

[12] Michael Shur. Wide band gap semiconductor technology: State-of-the-art. *Solid-State Electronics*, 155:65–75, 2019.

[13] H. Morkoc, S. Strite, G. B. Gao, M. E. Lin, B. Sverdlov, and M. Burns. Large-band-gap SiC, III-V nitride, and II-VI ZnSe-based semiconductor device technologies. *Journal of Applied physics*, 76(3):1363–1398, 1994.

[14] M. Razeghi and R. McClintock. A review of III-nitride research at the Center for Quantum Devices. *Journal of crystal growth*, 311(10):3067–3074, 2009.

[15] A. Khan and K. Balakrishnan. III-nitride-based short-wavelength ultraviolet light sources. 2011.

[16] A. L. Hicks, T. L. Theis, and M. L. Zellner. Emergent effects of residential lighting choices: prospects for energy savings. *Journal of Industrial Ecology*, 19(2):285–295, 2015.

[17] J. Y. Tsao and P. Waide. The world's appetite for light: empirical data and trends spanning three centuries and six continents. *Leukos*, 6(4):259–281, 2010.

[18] M. Elbuluk and N. R. N. Idris. The role power electronics in future energy systems and green industrialization. In *2008 IEEE 2nd International Power and Energy Conference*, pages 1–6. IEEE, 2008.

[19] Rohm Semiconductors. Sic power devices and modules - application note. [online], URL: https://d1d2qsbl8m0m72.cloudfront.net/en/products/databook/applinote/discrete/sic/common/sic-appli-e.pdf, Last visited 16.3.2020.

[20] H. R. Chang, R. N. Gupta, C. Winterhalter, and E. Hanna. Comparison of 1200 V silicon carbide Schottky diodes and silicon power diodes. In *Collection of Technical Papers. 35th Intersociety Energy Conversion Engineering Conference and Exhibit (IECEC)(Cat. No. 00CH37022)*, volume 1, pages 174–179. IEEE, 2000.

[21] S. Chowdhury, Z. Stum, Z. D. Li, K. Ueno, and T. P. Chow. Comparison of 600 V Si, SiC and GaN power devices. In *Materials Science Forum*, volume 778, pages 971–974. Trans Tech Publ, 2014.

[22] A. A. Arendarenko, V. A. Oreshkin, Y. N. Sveshnikov, and I. N. Tsyplenkov. Trends in the development of the epitaxial nitride compounds technology. *Modern Electronic Materials*, 2(2):33–40, 2016.

[23] Y. Zou, Y. Zhang, Y. Hu, and H. Gu. Ultraviolet detectors based on wide bandgap semiconductor nanowire: A review. *Sensors*, 18(7):2072, 2018.

[24] P. Schreiber, T. Dang, T. Pickenpaugh, G. A. Smith, P. Gehred, and C. W. Litton. Solar-blind UV region and UV detector development objectives. In *Photodetectors: Materials and Devices IV*, volume 3629, pages 230–248. International Society for Optics and Photonics, 1999.

[25] A. Gonzalez-Perez, K. M. Persson, and L. Samuelson. Semiconductor eco-materials for water treatment. 2019.

[26] A. Mills, R. H. Davies, and D. Worsley. Water purification by semiconductor photocatalysis. *Chemical Society Reviews*, 22(6):417–425, 1993.

[27] Y. Li, F. Chen, R. He, Y. Wang, and N. Tang. Semiconductor photocatalysis for water purification. In *Nanoscale Materials in Water Purification*, pages 689–705. Elsevier, 2019.

[28] S. Zhao, H. P. T. Nguyen, M. G. Kibria, and Z. Mi. III-nitride nanowire optoelectronics. *Progress in Quantum Electronics*, 44:14–68, 2015.

[29] P. Li and X. Meng. Thermal annealing effects on the optoelectronic characteristics of fully nanowire-based UV detector. *Journal of Materials Science: Materials in Electronics*, 27(7):7693–7698, 2016.

[30] F. Liu, L. Li, T. Guo, H. Gan, X. Mo, J. Chen, S. Deng, and N. Xu. Investigation on the photoconductive behaviors of an individual AlN nanowire under different excited lights. *Nanoscale research letters*, 7(1):454, 2012.

[31] C. Zhao, N. Alfaraj, R. Ch. Subedi, J. W. Liang, A. A. Alatawi, A. A. Alhamoud, M. Ebaid, M. S. Alias, T. K. Ng, and B. S. Ooi. III-nitride nanowires on unconventional substrates: From materials to optoelectronic device applications. *Progress in Quantum Electronics*, 61:1–31, 2018.

[32] T. Kente and S. D. Mhlanga. Gallium nitride nanostructures: Synthesis, characterization and applications. *Journal of Crystal Growth*, 444:55–72, 2016.

[33] M. H. Kane and N. Arefin. Gallium nitride on silicon substrates for LEDs. In *Nitride Semiconductor Light-Emitting Diodes*, pages 99–143. Elsevier, 2014.

[34] S. Strite and H. Morkoç. GaN, AlN, and InN: a review. *Journal of Vacuum Science & Technology B: Microelectronics and Nanometer Structures Processing, Measurement, and Phenomena*, 10(4):1237–1266, 1992.

[35] J. Neugebauer and C. G. Van de Walle. Gallium vacancies and the yellow luminescence in GaN. *Applied Physics Letters*, 69(4):503–505, 1996.

[36] M. A. Reshchikov, H. Morkoc, S. S. Park, and K. Lee. Yellow and green luminescence in a freestanding GaN template. *Applied Physics Letters*, 78(20):3041–3043, 2001.

[37] I. Vurgaftman, J. Meyer, and L. Ram-Mohan. Band parameters for III–V compound semiconductors and their alloys. *Journal of applied physics*, 89(11):5815–5875, 2001.

[38] M. E. Levinshtein, S. L. Rumyantsev, and M. S. Shur. *Properties of Advanced Semiconductor Materials: GaN, AlN, InN, BN, SiC, SiGe*. John Wiley & Sons, 2001.

[39] A. S. Augustine Fletcher and D. Nirmal. A survey of gallium nitride HEMT for RF and high power applications. *Superlattices and Microstructures*, 109:519–537, 2017.

[40] J. Maniš, J. Mach, M. Bartošík, T. Šamořil, Michal Horak, V. Čalkovský, D. Nezval, L. Kachtik, M. Konečny, and T. Šikola. Low temperature 2D GaN growth on Si (111) 7x7 assisted by hypethermal nitrogen ions. *Nanoscale Advances*, 4:3549–3556, 2022.

[41] A. Rothman, J. Maniš, V. G. Dubrovskii, T. Šikola, J. Mach, and E. Joslevich. Kinetics of guided growth of horizontal GaN nanowires on flat and faceted sapphire surfaces. *Nanomaterials*, 11(3):624, 2021.

[42] P. Blake, E. W. Hill, A. H. Castro Neto, K. S. Novoselov, D. Jiang, R. Yang, T. J. Booth, and A. K. Geim. Making graphene visible. *Applied physics letters*, 91(6):063124, 2007.

[43] J. Mach, J. Piastek, J. Maniš, V. Čalkovský, T. Šamořil, J. Damková, M. Bartošík, S. Voborný, M. Konečný, and T. Šikola. Low temperature selective growth of GaN single crystals on pre-patterned Si substrates. *Applied Surface Science*, 497:143705, 2019.

[44] J. W. Gerlach, T. Ivanov, L. Neumann, T. Hoche, D. Hirsch, and B. Rauschenbach. Epitaxial GaN films by hyperthermal ion-beam nitridation of Ga droplets. *Journal of Applied Physics*, 111(11):113521, 2012.

[45] P. Procházka. Fabrication of graphene and study of its physical properties. *PhD these, Brno University of Technology*, 2018.

[46] M. Leszczynski, H. Teisseyre, T. Suski, I. Grzegory, M. Bockowski, J. Jun, S. Porowski, K. Pakula, J. M. Baranowski, C. T. Foxon, et al. Lattice parameters of gallium nitride. *Applied Physics Letters*, 69(1):73–75, 1996.

[47] Chris G. Van de Walle. Effects of impurities on the lattice parameters of GaN. *Physical Review B*, 68(16):165209, 2003.

[48] Y. Gao and S. Okada. Energetics and electronic structures of thin films and heterostructures of a hexagonal GaN sheet. *Japanese Journal of Applied Physics*, 56(6):065201, 2017.

[49] A. Onen, D. Kecik, E. Durgun, and S. Ciraci. GaN: From three- to two-dimensional single-layer crystal and its multilayer van der Waals solids. *Physical Review B*, 93(8):085431, 2016.

[50] A. Onen, D. Kecik, E. Durgun, and S. Ciraci. Onset of vertical bonds in new GaN multilayers: beyond van der Waals solids. *Nanoscale*, 10(46):21842–21850, 2018.

[51] D. Xu, H. He, R. Pandey, and S. P. Karna. Stacking and electric field effects on the electronic properties of the layered GaN. *arXiv preprint arXiv - 1302.5157*, 2013.

[52] V. Darakchieva, P. P. Paskov, T. Paskova, E. Valcheva, B. Monemar, and M. Heuken. Lattice parameters of GaN layers grown on a-plane sapphire: Effect of in-plane strain anisotropy. *Applied physics letters*, 82(5):703–705, 2003.

[53] Celal Yelgel. First-principles modeling of GaN/MoSe van der Waals heterobilayer. *Turkish Journal of Physics*, 41(5):463–468, 2017.

[54] V. G. Dubrovskii, N. V. Sibirev, J. C. Harmand, and F. Glas. Growth kinetics and crystal structure of semiconductor nanowires. *Physical Review B*, 78(23):235301, 2008.

[55] A. Rothman, V. G. Dubrovskii, and E. Joselevich. Kinetics and mechanism of planar nanowire growth. *Proceedings of the National Academy of Sciences*, 117(1):152–160, 2020.

[56] V. G. Dubrovskii, N. V. Sibirev, G. E. Cirlin, I. P. Soshnikov, W. H. Chen, R. Larde, E. Cadel, P. Pareige, T. Xu, B. Grandidier, et al. Gibbs-thomson and diffusion-induced

contributions to the growth rate of Si, InP, and GaAs nanowires. *Physical Review B*, 79(20):205316, 2009.